

# Affleck-Kennedy-Lieb-Tasaki state on a honeycomb lattice is a universal quantum computational resource

Tzu-Chieh Wei, Ian Affleck, and Robert Raussendorf

Department of Physics and Astronomy, University of British Columbia, Vancouver, British Columbia V6T 1Z1, Canada

(Dated: January 13, 2013)

Universal quantum computation can be achieved by simply performing single-qubit measurements on a highly entangled resource state, such as cluster states. The family of Affleck-Kennedy-Lieb-Tasaki (AKLT) states has recently been intensively explored and shown to provide restricted computation. Here, we show that the two-dimensional AKLT state on a honeycomb lattice is a universal resource for measurement-based quantum computation.

PACS numbers: 03.67.Lx, 75.10.Jm, 64.60.ah

**Introduction.** Quantum computation promises exponential speedup over classical computation by exploiting the quantum mechanical nature of physical processes [1]. In addition to the standard circuit model based on unitary evolution, surprisingly, local measurement alone provides the same power of computation, given only a prior sufficiently entangled state [2, 3]. For this model of measurement-based quantum computation (MBQC), universal resource states are known to be very rare [4], but examples do exist [5–8]. The 2D cluster state on the square lattice is a universal resource state [2, 5]. Cluster states can be created by the Ising interaction from unentangled states [5, 9], but they do not arise as unique ground states of two-body interacting Hamiltonians [10]. However, by careful design of Hamiltonians, certain ground states can be used for universal MBQC [11, 12], and this opens up an appealing possibility of creating universal resource states by cooling.

A new perspective on MBQC emerged when it was discovered that the one-dimensional Affleck-Kennedy-Lieb-Tasaki (AKLT) state [13], originally constructed in the setting of condensed matter physics, can serve as resources for restricted computations [6, 14, 15]. In any dimension, the AKLT state is the ground state of a particularly simple Hamiltonian which only has nearest-neighbor two-body interactions, is rotationally invariant in spin space and shares all spatial symmetries of the underlying lattice [16]. The discovery of the resourcefulness of AKLT states creates additional avenues for its experimental realization [17], and has instilled novel concepts in MBQC, such as the renormalization group and the holographic principle [18, 19]. However, to date one crucial element was missing in this direction: the AKLT family was not known to contain a *universal* resource. Here, we overcome this gap by demonstrating that the AKLT state on a two-dimensional honeycomb lattice is a universal resource for measurement-based quantum computation.

To do this, we proceed in three steps. First, we show that it can be mapped to a random planar graph state  $|G(\mathcal{A})\rangle$  by local generalized measurement, with the graph  $G(\mathcal{A})$  depending on the set  $\mathcal{A}$  of measurement outcomes on all sites (defined below). Second, we argue that the computational universality of a typical resulting graph

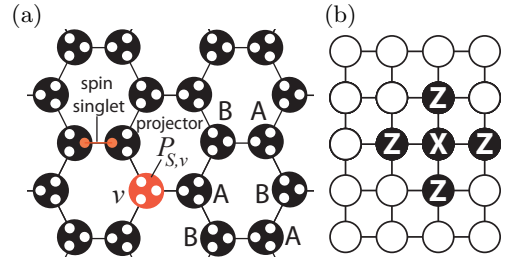


FIG. 1: Illustrations of the AKLT state and the 2D cluster state. (a) AKLT state. Spin singlets of two virtual spins 1/2 (i.e. qubits) are located on the edges of the honeycomb lattice. A projection  $P_{S,v}$  at each lattice site  $v$  onto the symmetric subspace of three virtual spins defines the AKLT state. In one hexagon, sites are labeled by  $A$  or  $B$  to show the bipartite (or bi-colorable) property of the honeycomb lattice. (b) 2D Cluster state. One qubit resides at each lattice site and one stabilizer generator is shown.

state  $|G(\mathcal{A})\rangle$  hinges solely on the connectivity of  $G(\mathcal{A})$ , and is thus a percolation problem. Third, we demonstrate via Monte Carlo simulation that the typical graphs  $G(\mathcal{A})$  are indeed deep in the supercritical phase.

The AKLT state [13] on the honeycomb lattice  $\mathcal{L}$  has one spin-3/2 per site of  $\mathcal{L}$ . The state space of each spin 3/2 can be viewed as the symmetric subspace of three virtual spin-1/2's, i.e., qubits. In terms of these virtual qubits, the AKLT state on  $\mathcal{L}$  is (see Fig. 1a)

$$|\Phi_{\text{AKLT}}\rangle \equiv \bigotimes_{v \in V(\mathcal{L})} P_{S,v} \bigotimes_{e \in E(\mathcal{L})} |\phi\rangle_e, \quad (1)$$

where  $V(\mathcal{L})$  and  $E(\mathcal{L})$  to denote the set of vertices and edges of  $\mathcal{L}$ , respectively.  $P_{S,v}$  is the projection onto the symmetric (equivalently, spin 3/2) subspace at site  $v$  of  $\mathcal{L}$  [20]. For an edge  $e = (v, w)$ ,  $|\phi\rangle_e$  denotes a singlet state, with one spin 1/2 at vertex  $v$  and the other at  $w$ .

A graph state  $|G\rangle$  is a stabilizer state [21] with one qubit per vertex of the graph  $G$  and is the unique eigenstate of a set of commuting operators [5], usually called the stabilizer generators [22],

$$X_v \bigotimes_{u \in \text{nb}(v)} Z_u |G\rangle = |G\rangle, \quad \forall v \in V(G), \quad (2)$$

POVM outcome	$z$	$x$	$y$
stabilizer generator	$\lambda_i \lambda_j Z_i Z_j$	$\lambda_i \lambda_j X_i X_j$	$\lambda_i \lambda_j Y_i Y_j$
$\bar{X}$	$\bigotimes_{j=1}^{3 C } X_j$	$\bigotimes_{j=1}^{3 C } Z_j$	$\bigotimes_{j=1}^{3 C } Z_j$
$\bar{Z}$	$\lambda_i Z_i$	$\lambda_i X_i$	$\lambda_i Y_i$

TABLE I: The dependence of stabilizers and encodings on the local POVM outcome.  $|C|$  denotes the total number of sites contained in a domain and  $i, j = 1 \dots 3|C|$ . The honeycomb lattice  $\mathcal{L}$  is bi-partite and all sites can be divided into either  $A$  or  $B$  sublattice,  $V(\mathcal{L}) = A \cup B$ ; see Fig. 1a. One choice of the sign is  $\lambda_i = 1$  if the virtual qubit  $i \in v \in A$  and  $\lambda_i = -1$  if  $i \in v' \in B$ ; this is due to the negative sign in the stabilizer generator for a singlet, i.e.,  $(-\sigma_{\mu,i} \sigma_{\mu,j})|\phi\rangle_{ij} = |\phi\rangle_{ij}$  for an edge  $(i, j)$ .

where  $\text{nb}(v)$  denotes the neighbors of vertex  $v$ , and  $X \equiv \sigma_x$ ,  $Y \equiv \sigma_y$  and  $Z \equiv \sigma_z$  are the Pauli matrices. A cluster state is a special case of graph states, with the underlying graph being a regular lattice (see Fig. 1b). Any 2D cluster state is a universal resource for measurement-based quantum computation [2, 23].

*Reduction to a graph state.* To show that the 2D AKLT state of four-level spin-3/2 particles can be converted to a graph state of two-level qubits, we need to preserve a local two-dimensional structure at each site. This is achieved by a local generalized measurement [1], also called positive-operator-value measure (POVM), on every site  $v$  on  $\mathcal{L}$ . The POVM consists of three rank-two elements

$$F_{v,z} = \sqrt{\frac{2}{3}}(|000\rangle\langle 000| + |111\rangle\langle 111|) \quad (3a)$$

$$F_{v,x} = \sqrt{\frac{2}{3}}(|+++ \rangle\langle +++| + |-- -- \rangle\langle -- --|) \quad (3b)$$

$$F_{v,y} = \sqrt{\frac{2}{3}}(|i,i,i\rangle\langle i,i,i| + |-i,-i,-i\rangle\langle -i,-i,-i|), \quad (3c)$$

where  $|0/1\rangle$ ,  $|\pm\rangle \equiv (|0\rangle \pm |1\rangle)/\sqrt{2}$  and  $|\pm i\rangle \equiv (|0\rangle \pm i|1\rangle)/\sqrt{2}$  are eigenstates of  $Z$ ,  $X$  and  $Y$ , respectively, and  $|0\rangle \equiv |\uparrow\rangle$ ,  $|1\rangle \equiv |\downarrow\rangle$ . Physically,  $F_{v,a}$  is proportional to a projector onto the two-dimensional subspace spanned by the  $S_a = \pm 3/2$  states. The above POVM elements obey the relation  $\sum_{\nu \in \{x,y,z\}} F_{v,\nu}^\dagger F_{v,\nu} = P_{S,v}$ , i.e., project onto the symmetric subspace, as required. The outcome  $a_v$  of the POVM at site  $v$  is random, which can be  $x, y$  or  $z$ , and it is correlated with the outcomes at other sites due to the entanglement in the AKLT state [13, 24]. As demonstrated below, the resulting quantum state, dependent on the random POVM outcomes  $\mathcal{A} = \{a_v, v \in V(\mathcal{L})\}$ ,

$$|\Psi(\mathcal{A})\rangle = \bigotimes_{v \in V(\mathcal{L})} F_{v,a_v} |\Phi_{\text{AKLT}}\rangle = \bigotimes_{v \in V(\mathcal{L})} F_{v,a_v} \bigotimes_{e \in E(\mathcal{L})} |\phi\rangle_e \quad (4)$$

is equivalent under local unitary transformations to an encoded graph state  $|\bar{G}(\mathcal{A})\rangle$ . We show that the corresponding graph  $G(\mathcal{A})$  is constructed from graph  $\mathcal{L}$  by applying the following two rules:

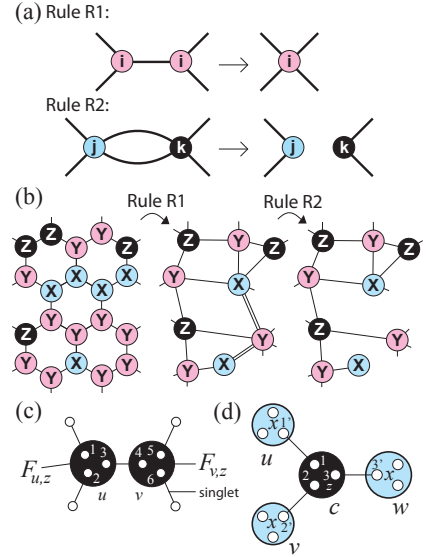


FIG. 2: Graphical rules for transformation of the lattice  $\mathcal{L}$  into the graph  $G(\mathcal{A})$ , depending on the POVM outcomes  $\mathcal{A}$ . a) Rules R1 and R2. b) An example of obtaining  $G(\mathcal{A})$ . The alphabets inside the circle indicate the POVM outcomes. c) An example to illustrate the qubit encoding of a domain. d) An example for demonstrating the stabilizer generator.

R1 (Edge contraction): Contract all edges  $e \in E(\mathcal{L})$  that connect sites with the same POVM outcome.

R2 (Mod-2 edge deletion): In the resultant multigraph, delete all edges of even multiplicity and convert all edges of odd multiplicity into conventional edges of multiplicity 1.

A set of sites in  $\mathcal{L}$  that are contracted into a single vertex of  $G(\mathcal{A})$  by rule R1 is called a *domain*. Each domain supports a single encoded qubit. The stabilizer generators and the encoded operators for the resulting codes are summarized in Table I.

Rule R1 derives intuitively from the antiferromagnetic property of the AKLT state: neighboring spin-3/2 particles must not have the same  $S_a = 3/2$  (or  $-3/2$ ) configuration [13]. Hence, after the projection onto  $S_a = \pm 3/2$  subspace by the POVM, the configurations for all sites inside a domain can only be  $|3/2, -3/2, \dots\rangle$  or  $|-3/2, 3/2, \dots\rangle$ , and these form the basis of a single qubit. This can also be understood in terms of the stabilizer. Consider the case where two neighboring POVMs yield the same outcome, say  $z$ ; see Fig. 2c. Due to the projections  $F_{u,z}$  and  $F_{v,z}$  (with  $u = \{1, 2, 3\}$  and  $v = \{4, 5, 6\}$  each containing three virtual qubits), the operators  $Z_1 Z_2$ ,  $Z_2 Z_3$ , and  $Z_4 Z_5$ ,  $Z_5 Z_6$  become stabilizer generators of  $|\Psi(\mathcal{A})\rangle$ . Moreover, the stabilizer  $-Z_3 Z_4$  of  $|\phi\rangle_{34}$  commutes with  $F_{u,z} \otimes F_{v,z}$ , and thus remains a stabilizer element for  $|\Psi(\mathcal{A})\rangle$  [20]. In brief, the stabilizer generators  $Z_1 Z_2, Z_2 Z_3, -Z_3 Z_4, Z_4 Z_5, Z_5 Z_6$  lead to a single encoded qubit

$$\alpha|(000)_u(111)_v\rangle + \beta|(111)_u(000)_v\rangle,$$

supported by the two sites  $u$  and  $v$  jointly. Note the antiferromagnetic ordering [13] among groups of three virtual qubits. To reduce the support of this logical qubit to an individual site, a measurement in the basis  $\{|(000)_v\rangle \pm |(111)_v\rangle\}$  is performed. The resulting state is  $\alpha|(000)_u\rangle \pm \beta|(111)_u\rangle$ , with the sign “ $\pm$ ” known from the measurement outcome. This is the proper encoding for a domain consisting of a single site. Domains of more than two sites are thereby reduced to single sites.

To see that  $|\Psi(\mathcal{A})\rangle$  is indeed equivalent under local unitary transformations to an encoded graph state  $|\overline{G(\mathcal{A})}\rangle$ , we consider the example of four domains  $c, u, v, w$ , each consisting of a single site of  $\mathcal{L}$ , where the POVM outcome is  $z$  on the central domain  $c$  and  $x$  on all lateral domains  $u, v$  and  $w$ ; see Fig. 2d. By similar arguments as above [20], the operator  $\mathcal{O} \equiv -X_1 X_{1'} X_2 X_{2'} X_3 X_{3'}$  is in the stabilizer of  $|\Psi(\mathcal{A})\rangle$ . Using the encoding in Table I, i.e., with the encoded Pauli operators  $\overline{X}_c = Z_1 Z_2 Z_3$ ,  $\overline{Z}_u = \pm X_{1'}$ ,  $\overline{Z}_v = \pm X_{2'}$ , and  $\overline{Z}_w = \pm X_{3'}$ , we find that  $\mathcal{O} = \pm \overline{X}_c \overline{Z}_u \overline{Z}_v \overline{Z}_w$  which is (up to a possible sign) one stabilizer generator defining the graph state; see Eq. (2).

By the above construction, if two domains  $u, v$  are connected by an edge of multiplicity  $m$ , the inferred graph state stabilizer generators will contain factors of  $\overline{X}_u \overline{Z}_v^m$  or  $\overline{X}_v \overline{Z}_u^m$ . Rule R2 thus follows the observation that  $Z^2 = I$ . Generalizing these ideas, one can rigorously prove that for any  $\mathcal{A}$  of POVM outcomes, the state  $|\Psi(\mathcal{A})\rangle$  is local-unitarily equivalent to an encoded graph state  $|\overline{G(\mathcal{A})}\rangle$  [25]. We shall denote by  $|G(\mathcal{A})\rangle$  the same graph state but with domains of single sites.

*Random graph states and percolation.* Whether or not typical graph states  $|G(\mathcal{A})\rangle$  are universal resources hinges solely on connectivity properties of  $G(\mathcal{A})$ , and is thus a percolation problem [26]. Specifically, for a large initial  $\mathcal{L}$  the random graph state  $|G(\mathcal{A})\rangle$  can, with close to unit probability, be efficiently reduced to a large two-dimensional cluster state if the following properties hold:

- C1 The distribution of the number of sites in a domain (i.e. domain size) is *microscopic*, i.e., the largest domain size can at most scale logarithmically with the total number of sites  $|V(\mathcal{L})|$  in the large  $\mathcal{L}$  limit.
- C2 The probability of the existence of a path through  $G(\mathcal{A})$  from the left to the right (or top to bottom) approaches unity in the limit of large  $\mathcal{L}$ .

Condition C1 ensures that the graph  $G(\mathcal{A})$  remains macroscopic if the original  $\mathcal{L}$  was, and Condition C2 ensures that the system is in the supercritical phase with a macroscopic spanning cluster.

Together with planarity, which holds for all graphs  $G(\mathcal{A})$  by construction, the conditions C1 and C2 are sufficient for the reduction of the random graph state to a standard universal cluster state. The proof [25] extends a similar result already established for site percolation on a square lattice [27]. The physical intuition comes from percolation theory. In the supercritical phase (where there exists a macroscopic spanning cluster and connects

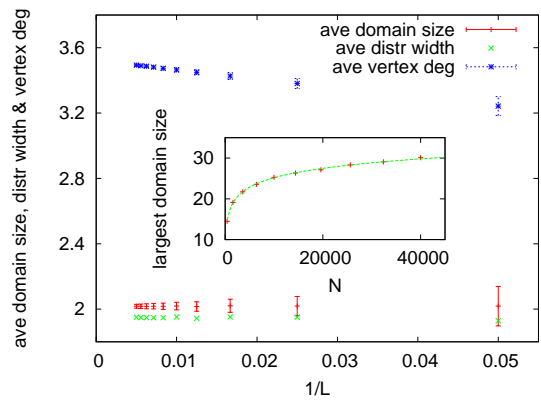


FIG. 3: (color online) Average domain size, average width of domain size distribution, average degree of a vertex, and the largest domain size (inset) in the typical graphs vs.  $L$ , with  $N = L^2$  being the total number of sites. For better discernibility, we suppress the errorbars for one set of data. The largest domain size scales with  $N$  as  $3.337 \ln(N) - 5.566$ .

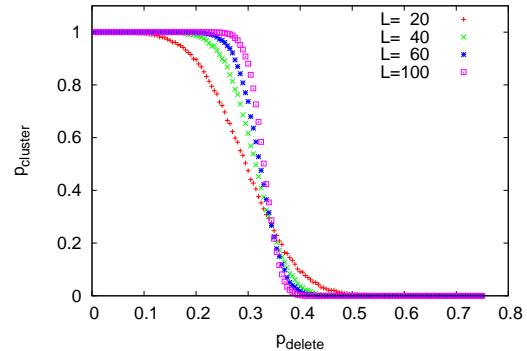


FIG. 4: (color online) Percolation study of the random graphs of domains: probability of a spanning cluster  $p_{\text{cluster}}$  vs. that to delete a vertex  $p_{\text{delete}}$ . The threshold for destroying the spanning cluster is around  $p_{\text{delete}} \approx 0.33$  in deleting vertices.

one boundary to the other), the spanning cluster contains a subgraph which is topologically equivalent to a coarse-grained two-dimensional lattice structure. This subgraph can be carved out and subsequently cleaned off all imperfections by local Pauli measurements, leading to a perfect two-dimensional lattice.

*Numerical results.* We used Monte Carlo simulations to sample typical random graphs resulting from the POVM and compute their properties. The simulations utilize a generalized Hoshen-Kopelman algorithm [28] to identify domains. Due to the entanglement in the AKLT state, the local POVM outcomes are correlated which is fully taken into account in our simulations. In particular, to sample typical POVM outcomes  $\mathcal{A}$  correctly, we use a Metropolis method to update configurations. For each site we attempt to flip the type (either  $x, y$  or  $z$ ) to one of the other two equally and accept the flip with a probability  $p_{\text{acc}} = \min\{1, 2^{|V'| - |\mathcal{E}'| - |V| + |\mathcal{E}|}\}$ , where  $|V|$  and  $|\mathcal{E}|$

denote the number of domains and inter domain edges, respectively, before the flip and Rule 2, and similarly  $|V'|$  and  $|\mathcal{E}'|$  for the flipped configuration [25].

We have analyzed lattices of size up to  $200 \times 200$  sites. The average degree of vertices in the typical random graphs is about 3.52(1), when extrapolated to an infinite system size. Furthermore, the typical random graphs retain large number of vertices  $|\bar{V}| = 0.495(2)N$ , edges  $|\bar{E}| = 0.872(4)N$ , and independent cycles (or the Betti number)  $\bar{B} = 0.377(2)N$ , where  $N = L \times L$  is the total number of sites in the initial honeycomb lattice. The size of the largest domain was never macroscopic and followed a logarithmic dependence on  $N$ . The average number of sites  $v \in V(\mathcal{L})$  contained in a typical domain, when extrapolated to the infinite system, is 2.02(1) and the width in the domain size distribution is extrapolated to 1.94(1). Our simulations show that condition C1 holds; see Fig. 3. For all POVM outcomes sampled, a macroscopic cluster existed, allowing a horizontal and a vertical traversing path through the resulting graphs  $G(\mathcal{A})$ . This shows that condition C2 holds.

**Robustness.** We now quantify how deep typical graphs  $G(\mathcal{A})$  are in the supercritical phase of the percolation transition. A first measure is the average vertex degree. A heuristic argument based on a branching process sug-

gests that a graph has a macroscopic connected component whenever the average vertex degree is  $\bar{d} > 2$  [29]. In our case, the typical graphs  $G(\mathcal{A})$  have an average degree of 3.52, suggesting that the system is deep in the supercritical phase. Furthermore, we randomly delete a fraction of vertices or edges from  $G(\mathcal{A})$ . On average, it requires a deletion probability as high as  $p_{\text{delete}}^* = 0.33(1)$  for vertices (see Fig. 4) and  $p_{\text{delete}}^* = 0.43(1)$  for edges (not shown) in order to the spanning cluster. These numbers demonstrate the robustness of the connectivity property.

**Concluding remarks.** We investigated MBQC on the AKLT states and established one crucial missing ingredient in this area: the two-dimensional spin-3/2 AKLT state on a honeycomb lattice is indeed a universal resource. The approach described in this work also applies to other trivalent lattices, such as the Archimedean lattices:  $(3, 12^2)$ ,  $(4, 6, 12)$  and  $(4, 8^2)$ , which have higher percolation thresholds than the honeycomb lattice.

After the completion of our work, we learned of a similar result by Miyake with a different approach [30].

**Acknowledgment.** This work was supported by NSERC, MITACS, CIFAR and the Sloan Foundation.

- 
- [1] M. Nielsen and I. Chuang, *Quantum Computation and Quantum Information* (Cambridge Univ. Press, 2000).
  - [2] R. Raussendorf and H. J. Briegel, Phys. Rev. Lett. **86**, 5188 (2001).
  - [3] H. J. Briegel et al., Nature Phys. **5**, 19 (2009).
  - [4] D. Gross, S.T. Flammia, and J. Eisert, Phys. Rev. Lett. **102**, 190501 (2009); M. Bremner, C. Mora, and A. Winter, *ibid* **102**, 190502 (2009).
  - [5] H. J. Briegel and R. Raussendorf, Phys. Rev. Lett. **86**, 910 (2001).
  - [6] D. Gross and J. Eisert, Phys. Rev. Lett. **98**, 220503 (2007).
  - [7] F. Verstraete and J. I. Cirac, Phys. Rev. A **70** 060302(R) (2004).
  - [8] J.-M. Cai et al., Phys. Rev. Lett. **103**, 050503 (2009).
  - [9] O. Mandel et al., Nature (London) **425**, 937 (2003).
  - [10] M. A. Nielsen, Rep. Math. Phys. **57**, 147 (2006).
  - [11] X. Chen et al., Phys. Rev. Lett. **102**, 220501 (2009).
  - [12] J.-M. Cai, A. Miyake, W. Dür, and H. J. Briegel, Phys. Rev. A **82**, 052309 (2010).
  - [13] I. Affleck, T. Kennedy, E. H. Lieb, and H. Tasaki, Phys. Rev. Lett. **59**, 799 (1987); I. Affleck, T. Kennedy, E. H. Lieb, and H. Tasaki, Comm. Math. Phys. **115**, 477 (1988).
  - [14] G. K. Brennen and A. Miyake, Phys. Rev. Lett. **101**, 010502 (2008).
  - [15] X. Chen, R. Duan, Z. Ji, and B. Zeng, Phys. Rev. Lett. **105**, 020502 (2010).
  - [16] With an appropriate choice of boundary conditions, the AKLT state is the unique ground state; see also Ref. cite-suppl. In contrast to 1D, the 2D AKLT state on the honeycomb lattice was only shown to possess exponentially decaying correlation functions [13], nevertheless suggesting a spectral gap.
  - [17] R. Kaltenbaek et al., Nature Phys. **6**, 850 (2010).
  - [18] A. Miyake, Phys. Rev. Lett. **105**, 040501 (2010).
  - [19] S. D. Bartlett, G. K. Brennen, A. Miyake, and J. M. Renes, Phys. Rev. Lett. **105**, 110502 (2010).
  - [20] See the supplemental material in the Appendix for further discussions.
  - [21] M. Hein, J. Eisert, and H.-J. Briegel, Phys. Rev. A **69**, 062311 (2004).
  - [22] D. Gottesman, *Stabilizer Codes and Quantum Error Correction*, Ph.D. Thesis, Caltech (1997).
  - [23] M. Van den Nest, A. Miyake, W. Dür, and H. J. Briegel, Phys. Rev. Lett. **97**, 150504 (2006).
  - [24] H. Katsura et al., J. Phys. A: Math. Theor. **43**, 255303 (2010).
  - [25] T.-C. Wei, I. Affleck, and R. Raussendorf, arXiv:1009.2840.
  - [26] R. Durrett, *Random Graph Dynamics*, Cambridge University Press (2007).
  - [27] D. E. Browne et al., New J. Phys. **10**, 023010 (2008).
  - [28] J. Hoshen and R. Kopelman, Phys. Rev. B **14**, 3438 (1976).
  - [29] This criterion, based on the critical degree  $d_c$ , is exact for random graphs of uniform degree [26]. It holds surprisingly well for lattice graphs, e.g., in honeycomb:  $d_c = 1.958$ , Kagome:  $d_c = 2.097$ , square:  $d_c = 2$ , triangular:  $d_c = 2.084$ .
  - [30] A. Miyake, arXiv:1009.3491v1.

### Appendix A: Projection onto the symmetric subspace of three qubits

The addition of angular momenta for three qubits (spin-1/2) gives rise to three subspaces:  $\frac{1}{2} \otimes \frac{1}{2} \otimes \frac{1}{2} = \frac{1}{2} \oplus \frac{1}{2} \oplus \frac{3}{2}$ . The four basis states of the  $S = 3/2$  subspaces are  $|3/2, 3/2\rangle$ ,  $|3/2, -3/2\rangle$ ,  $|3/2, 1/2\rangle$  and  $|3/2, -1/2\rangle$  (with the quantization axis being assumed to be  $z$ ), and they can be expressed in terms of the three-qubit basis states (with  $|0/1\rangle \equiv |\uparrow/\downarrow\rangle = |1/2, \pm 1/2\rangle$ )

$$|3/2, 3/2\rangle = |000\rangle, \quad |3/2, -3/2\rangle = |111\rangle, \quad (\text{A1a})$$

$$|3/2, 1/2\rangle = |W\rangle \equiv \frac{1}{\sqrt{3}}(|001\rangle + |010\rangle + |100\rangle), \quad (\text{A1b})$$

$$|3/2, -1/2\rangle = |\bar{W}\rangle \equiv \frac{1}{\sqrt{3}}(|110\rangle + |101\rangle + |011\rangle). \quad (\text{A1c})$$

As can be clearly seen, states in this subspace are symmetric under permutation of the three qubits and the corresponding projection operator is

$$P_{S,v} \equiv |000\rangle\langle 000| + |W\rangle\langle W| + |\bar{W}\rangle\langle \bar{W}| + |111\rangle\langle 111|. \quad (\text{A2})$$

*The POVM and the post-POVM state.* To show that the 2D AKLT state of four-level spin-3/2 particles can be converted to a graph state of two-level qubits, we need to preserve a local two-dimensional structure at each site. This is achieved by a local generalized measurement [1], also called positive-operator-value measure (POVM), on every site  $v$  on  $\mathcal{L}$ . The POVM consists of three rank-two elements  $F_{v,a}^\dagger F_{v,a}$  with  $a = x, y$ , or  $z$ , and

$$F_{v,z} = \sqrt{\frac{2}{3}}(|000\rangle\langle 000| + |111\rangle\langle 111|) \quad (\text{A3a})$$

$$F_{v,x} = \sqrt{\frac{2}{3}}(|+++\rangle\langle +++| + |--\rangle\langle --|) \quad (\text{A3b})$$

$$F_{v,y} = \sqrt{\frac{2}{3}}(|i, i, i\rangle\langle i, i, i| + |-i, -i, -i\rangle\langle -i, -i, -i|), \quad (\text{A3c})$$

where  $|0/1\rangle$ ,  $|\pm\rangle \equiv (|0\rangle \pm |1\rangle)/\sqrt{2}$  and  $|\pm i\rangle \equiv (|0\rangle \pm i|1\rangle)/\sqrt{2}$  are eigenstates of the three Pauli operators  $Z$ ,  $X$  and  $Y$ , respectively. Physically,  $F_{v,a}$  is proportional to a projector onto the two-dimensional subspace spanned by the  $S_a = \pm 3/2$  states, i.e.,

$$F_{v,a} = \sqrt{\frac{2}{3}}(|3/2, +3/2\rangle_a\langle 3/2, +3/2| + |3/2, -3/2\rangle_a\langle 3/2, +3/2|), \quad (\text{A4})$$

with  $\hat{S}_a|3/2, \pm 3/2\rangle_a = \pm 3/2|3/2, \pm 3/2\rangle_a$  and  $a$  indicating the quantization axis.

The above POVM elements obey the relation  $\sum_{\nu \in \{x, y, z\}} F_{v,\nu}^\dagger F_{v,\nu} = P_{S,v} = \mathbb{1}_{S=3/2}$ , i.e., project onto the symmetric subspace, as required. The outcome  $a_v$  of the POVM at site  $v$  is random, which can be  $x$ ,  $y$  or  $z$ . The resulting quantum state, dependent on the random POVM outcomes  $\mathcal{A} = \{a_v, v \in V(\mathcal{L})\}$ ,

$$|\Psi(\mathcal{A})\rangle = \bigotimes_{v \in V(\mathcal{L})} F_{v,a_v} |\Phi_{\text{AKLT}}\rangle = \bigotimes_{v \in V(\mathcal{L})} F_{v,a_v} \bigotimes_{e \in E(\mathcal{L})} |\phi\rangle_e, \quad (\text{A5})$$

where  $|\phi\rangle_e$  denotes a singlet state  $(|01\rangle - |10\rangle)/\sqrt{2}$  on the edge  $e$ .

*Example 1: qubit encoding.* Consider the case where two neighboring POVMs yield the same outcome, say  $z$ ; see Fig. 2c in the main text. Due to the projections  $F_{u,z}$  and  $F_{v,z}$  (with  $u = \{1, 2, 3\}$  and  $v = \{4, 5, 6\}$  each containing three virtual qubits), the operators  $Z_1 Z_2$ ,  $Z_2 Z_3$ , and  $Z_4 Z_5$ ,  $Z_5 Z_6$  become stabilizer generators of  $|\Psi(\mathcal{A})\rangle$ , as, e.g.,

$$Z_1 Z_2 F_{u,z} = F_{u,z} \quad (\text{A6})$$

and hence

$$Z_1 Z_2 |\Psi(\mathcal{A})\rangle = Z_1 Z_2 \bigotimes_{v \in V(\mathcal{L})} F_{v,a_v} \bigotimes_{e \in E(\mathcal{L})} |\phi\rangle_e = |\Psi(\mathcal{A})\rangle. \quad (\text{A7})$$

Moreover, the stabilizer  $-Z_3Z_4$  of  $|\phi\rangle_{34}$  (i.e.,  $-Z_3Z_4|\phi\rangle_{34} = |\phi\rangle_{34}$ ) commutes with  $F_{u,z} \otimes F_{v,z}$ , and thus remains a stabilizer element for  $|\Psi(\mathcal{A})\rangle$ ,

$$-Z_3Z_4|\Psi(\mathcal{A})\rangle = \bigotimes_{v \in V(\mathcal{L})} F_{v,a_v}(-Z_3Z_4) \bigotimes_{e \in E(\mathcal{L})} |\phi\rangle_e = |\Psi(\mathcal{A})\rangle. \quad (\text{A8})$$

Therefore, regarding sites  $u$  and  $v$ ,  $|(000)_u(111)_v\rangle$  and  $|(111)_u(000)_v\rangle$  are the only two basis states that are stabilized (i.e., common eigenstates with eigenvalue equal to unity) by the above five operators,  $Z_1Z_2, Z_2Z_3, -Z_3Z_4, Z_4Z_5, Z_5Z_6$ . This leads to a single encoded qubit

$$\alpha|(000)_u(111)_v\rangle + \beta|(111)_u(000)_v\rangle, \quad (\text{A9})$$

supported by the two sites  $u$  and  $v$  jointly. If more neighboring sites share the same POVM outcome, the encoded qubit can be easily extended.

*Example 2: graph-state stabilizer generator.* To see that  $|\Psi(\mathcal{A})\rangle$  is indeed equivalent under local unitary transformations to an encoded graph state  $|\overline{G(\mathcal{A})}\rangle$ , we consider the example of four domains  $c, u, v, w$ , each consisting of a single site of  $\mathcal{L}$ , where the POVM outcome is  $z$  on the central domain  $c$  and  $x$  on all lateral domains  $u, v$  and  $w$ ; see Fig. 2d of the main text. By direct computation we have that

$$[-X_1X_{1'}, F_{u,x}] = [-X_2X_{2'}, F_{v,x}] = [-X_3X_{3'}, F_{w,x}] = 0. \quad (\text{A10})$$

Although  $-X_iX_{i'}$  individually does not commute with  $F_{c,z}$ , the operator  $\mathcal{O} \equiv X_1X_{1'}X_2X_{2'}X_3X_{3'}$  does, as by direction computation,

$$X_1X_2X_3(|000\rangle\langle 000| + |111\rangle\langle 111|) = |111\rangle\langle 000| + |000\rangle\langle 111| = (|000\rangle\langle 000| + |111\rangle\langle 111|)X_1X_2X_3, \quad (\text{A11})$$

we have

$$[X_1X_2X_3, F_{c,z}] = 0. \quad (\text{A12})$$

This shows that  $\mathcal{O}$  is in the stabilizer of  $|\Psi(\mathcal{A})\rangle$ , i.e.,  $\mathcal{O}|\Psi(\mathcal{A})\rangle = |\Psi(\mathcal{A})\rangle$ . Using the encoding in Table 1 of the main text, i.e., with the encoded Pauli operators  $\overline{X}_c = Z_1Z_2Z_3$ ,  $\overline{Z}_u = X_{1'}$ ,  $\overline{Z}_v = X_{2'}$ , and  $\overline{Z}_w = X_{3'}$ , we find that  $\mathcal{O} = \overline{X}_c\overline{Z}_u\overline{Z}_v\overline{Z}_w$  which is (up to a possible sign) one stabilizer generator defining the graph state.

*The Hamiltonian and boundary conditions.* The construction of the AKLT state by the valence-bond picture gives rise to a state that is the ground state of the following Hamiltonian

$$H = \sum_{\text{edge } \langle i,j \rangle} \hat{P}_{i,j}^{(S=3)} = \sum_{\text{edge } \langle i,j \rangle} \left[ \vec{S}_i \cdot \vec{S}_j + \frac{116}{243}(\vec{S}_i \cdot \vec{S}_j)^2 + \frac{16}{243}(\vec{S}_i \cdot \vec{S}_j)^3 + \frac{55}{108} \right], \quad (\text{A13})$$

where  $\hat{P}_{i,j}^{(S=3)}$  is a projector of the neighboring sites  $i$  and  $j$  onto a total  $S = 3$  subspace. In the case of the periodic boundary condition, the AKLT is the unique ground state. In the case of the open boundary condition, one can terminate every boundary spin-3/2 by a spin-1/2, and add a corresponding term in the Hamiltonian,

$$h_{i,i'} = P_{i,i'}^{(S=2)} = \frac{1}{2}\vec{S}_i \cdot \vec{s}_{i'} + \frac{5}{4}, \quad (\text{A14})$$

where  $\vec{S}_i$  is the spin-3/2 operator at the boundary and  $\vec{s}_{i'}$  is the associated spin-1/2 operator. These additional Hamiltonian terms for all boundary pairs make the AKLT state a unique ground state.

In the case of the open boundary condition, the planarity of the graph is preserved even after the POVMs. However, in the case of the periodic boundary condition, the underlying topology is that of a torus. To make the graph of the corresponding graph state after the POVMs be planar, one simply measures the logical  $Z$  on sites along the two independent cycles and this will cut the torus into a plane.

---